NUREG/CR-3643
SAND83-2493
RV
Printed April 1984

Heterogeneous Oxidative Degradation in Irradiated Polymers

R. L. Clough, K. T. Gillen, C. A. Quintana

Prepared by
Sandia National Laboratories
Albuquerque, New Mexico 87185 and Livermore, California 94550
for the United States Department of Energy
under Contract DE-AC04-76DP00789

Prepared for
U. S. NUCLEAR REGULATORY COMMISSION

Available from

GPO Sales Program
Division of Technical Information and Document Control
U.S. Nuclear Regulatory Commission
Washington, D.C. 20555

and

National Technical Information Service
Springfield, Virginia 22161

NUREG/CR-3643
SAND83-2493
RV

HETEROGENEOUS OXIDATIVE DEGRADATION IN IRRADIATED POLYMERS

R. L. Clough, K. T. Gillen, and C. A. Quintana

April 1984

Sandia National Laboratories
Albuquerque, NM 87185
Operated by
Sandia Corporation
for the
U.S. Department of Energy

Prepared for
Division of Engineering Technology
Office of Nuclear Regulatory Research
U.S. Nuclear Regulatory Commission
Washington, DC 20555
Under Memorandum of Understanding DOE 40-550-75
NRC FIN No.A-1051

ABSTRACT

When polymeric materials are irradiated in the presence of air, oxygen-diffusion effects can, depending upon dose rate, lead to oxidative degradation which occurs only near the edges. This report describes the use of several recently developed techniques which are of general use for studying heterogeneous degradation in commercial polymeric materials. The techniques discussed are: optical evaluation of cross-sectioned, polished samples; cross-sectional profiling of changes in relative hardness; and profiling of density changes. Oxidation penetration depths are given for a number of major polymer types as a function of dose rate. A detailed example is given graphically illustrating the effects of differing oxidative penetration depths on the radiation-degradation behavior of a Viton® O-ring material; this particular material becomes hard and brittle when irradiated at high dose rate, but soft and stretchable when irradiated at low dose rates.

The data presented show examples for several materials where the accelerated "age" is strongly influenced by environment application (e.g., dose-rate effects), or where the use of an overstress approach (i.e., effectively a large "margin" in total dose) cannot compensate for the effect of dose-rate. The techniques discussed in this report can aid in the determination of such effects and their magnitude and in the selection of appropriate accelerated aging methods. With such knowledge about material degradation, and with aging methods selected on these data-based approaches, there can be increased assurance that equipment qualification procedures are adequate.

CONTENTS

LIST OF FIGURES

LIST OF TABLES

ACKNOWLEDGMENT

The authors are grateful to D. Tallant and K. Higgins who performed the laser experiments, and to D. Mitchell who performed permeation measurements.

EXECUTIVE SUMMARY

Polymeric materials may undergo oxygen-diffusion-limited, heterogeneous degradation with significant oxidation occurring only near the surfaces. It is important in studying polymer degradation (and in designing accelerated aging experiments) to be able to determine under what conditions heterogeneous degradation occurs, and to estimate the extent of significant oxidative penetration under those conditions. We describe here the use of several techniques for quick identification of oxidative degradation gradients. One determination of oxidation depth is accomplished by optical examination of metallographically polished cross-sectioned samples; oxidized and nonoxidized regions are distinguished by differences in surface reflectivity. A more detailed determination of the shapes of degradation gradients is accomplished by performing a series of sensitive determinations of relative hardness changes across the surface of cross-sectioned, polished samples. Typical oxidation depths for the commercial polymers examined are on the order of fractions of millimeters over a dose-rate range of 10^4-10^6 rads/h. Significant variations among different materials are found, as would be expected given differences in oxygen consumption and permeation rates.

A detailed example is given of the tensile property behavior of a Viton® material over a range of dose rates where the degradation is seen to change from strongly heterogeneous at high dose rates to homogeneous as the dose rate is lowered. Degradation differences in this material are very pronounced. At high dose rates the polymer undergoes primarily cross-linking to give a hard brittle material, whereas under lower dose rates, where oxygen permeation is complete, the polymer undergoes predominantly scission to yield a soft, stretchable material.

The data presented show examples for several materials where the accelerated "age" is strongly influenced by environment application (e.g., dose-rate effects), or where the use of an overstress approach (i.e., effectively a large "margin" in total dose) cannot compensate for the effect of dose-rate. The techniques discussed in this report can aid in the determination of such effects and their magnitude and in the selection of appropriate accelerated aging methods. With such knowledge about material degradation, and with aging methods selected on these data-based approaches, there can be increased assurance that equipment qualification procedures are adequate.

INTRODUCTION

Elucidation of the fundamental chemical and physical changes which occur in polymeric materials as they undergo degradation in various environments has been a major topic of continuing research in polymer science. One factor which can be crucial to understanding the deterioration of polymer properties is the occurrence of heterogeneous degradation in bulk polymers. Heterogeneous degradation can result from numerous factors and can arise in many different environments.

Diffusion processes are a major cause of heterogeneous degradation. The diffusion of oxygen into a polymer undergoing oxidative degradation can be a rate-limiting step causing the material to become oxidized only near the edges. In air environments, oxidation is a common degradation mechanism, and oxidation gradients may arise in materials exposed to ultraviolet light, elevated temperature, high-energy radiation, or mechanical stress. Radiation oxidation is known to be an important degradation mechanism for organic polymers in a nuclear environment, as in a reactor containment building. This report discusses oxidation gradients which arise as a result of exposure to high-energy radiation.

The fact that heterogeneous radiation-induced oxidation can occur was recognized by the earliest workers who irradiated polymers in the presence of air,[1-4] and the existence of this phenomenon has been mentioned in numerous articles.[5-9] Heterogeneous degradation may occur under the ambient application environment in which a material is used. It can also occur in accelerated aging tests, where the size of the oxidized region can depend on the stress level used in the experiment.

In the course of our work on developing accelerated radiation aging techniques to understand long-term polymer degradation in air environments,[10-17] it became apparent that an understanding of macroscopic material properties as a function of radiation exposure in air-containing environments would require a knowledge of (1) the dose rates at which inhomogeneous oxidation occurs for a given material of given thickness, and (2) the depth of significant oxidation under conditions where such gradients occur.[16] Relatively few studies of heterogeneous oxidation have been done. Although several workers have observed oxidative heterogeneities by cutting up samples and analyzing the pieces using such techniques as infrared spectroscopy, solubility, and molecular weight determination, these techniques are of limited utility for numerous commercial materials which are

often cross-linked and spectroscopically complicated. Consequently, very little quantitative data has been presented on the depth of oxidative degradation in bulk polymers as a function of radiation conditions. Indeed, most studies of radiation effects on polymers in the presence of oxygen have been carried out on samples in the form of powders or very thin films so as to avoid the "complication" of diffusion effects.

One interesting technique applicable to special cases has been described for observing oxidation. Seguchi and coworkers prepared samples of clear polyethylene containing a dye.[18] Upon irradiation under different pressures of atmospheric oxygen, it was possible to identify the extent of oxygen penetration based on the fact that the oxidized dye changed color. We have sought to develop more general means for identifying gradients in a wide spectrum of commercial polymer types. This report describes the use of simple techniques applicable to such materials which allow rapid identification of oxidative degradation heterogeneities. Results on the depth of significant oxidative degradation for a number of polymeric materials exposed to radiation environments are presented. The effect of differing oxidation depths on the mechanical properties of degraded samples of one material, Viton®, is discussed in detail.

The significance of this work to determining a particular and adequate accelerated-aging method is severalfold. First the data presented show clear examples that the fundamental degradation modes of materials must be understood for proper accelerated-aging method selection. Second, the techniques discussed can be used to screen for heterogeneous degradation effects; if observed, it should be possible to adjust the aging method to eliminate the heterogeneity. Third, in one example, it is shown how the concept of overstressing one environmental parameter (radiation) may not account for the dose-rate effect; this is an example where a "margin" concept may not apply.

This report emphasizes the importance of an adequate data base and an understanding of material degradation phenomenology to the selection of an appropriate aging method.

EXPERIMENTAL

Test specimens were cut from samples of commercial polymeric materials. Irradiation was carried out in Sandia's Co-60 facility which has been described elsewhere.[14] Throughout the irradiation, a steady flow of air was supplied to the sample chambers at a rate approximately equivalent to two changes of atmosphere per hour. Tensile tests were performed using a Model 1130 Instron with an electrical tape extensometer clamped to the sample. Samples were

strained at 12.7 cm/min with an initial jaw gap of 5.1 cm. Elongation at break and ultimate tensile strength were measured at 23°C.

For optical determinations of oxidation depth, cross sections of irradiated samples were potted in Shell Epon 828 epoxy and cured overnight at 90°C with a diethanolamine catalyst. The samples were polished using standard metallographic techniques;[19,20] the epoxy-mounted specimens were ground on 120 through 600 grit silicon carbide abrasive papers, and then successively polished on nylon cloths using 30, 6, and 1 micron diamond paste. Photographs shown in the report were obtained with a Leitz Metallograph with bright-field illumination at a magnification of 18. Measurements of the oxidized areas in samples were obtained using a microscope fitted with a filar eyepiece.

For probe penetration measurements, cross-sectioned polymers were placed in a specially designed vise constructed of a hollowed-out cylinder of rigid plastic material (2.5 cm diameter) having adjustable, opposing screws which are used to push 2 metal plates towards the center of the vise. Three samples of cross-sectioned polymer were held together between the plates. The entire vise assembly, with samples in place, was subjected to standard metallographic polishing steps as described above. Tests were performed across the (cross-sectioned) surface of the central of the three samples. The measurements were accomplished by determining the displacement of a weighted probe into a polymer sample. The samples were placed on a calibrated X-Y translational microscope stage, and typical measurements were made at regular intervals of between .05 and .15 mm. To provide a small probe tip for measurements of the desired resolution, a conical diamond phonograph needle having a tip angle of 60° was affixed to the shank of a micro drill bit, which was itself attached to the shaft of a commercial probe used for the Perkin Elmer TMS-1 Thermomechanical Analyzer. The LVDT, loading stage, and electronics of this commercial instrument were utilized to measure penetration distances. The diamond-tipped probe was first preloaded with approximately 0.5 g for 30 sec, then an additional load of either 3 g or 5 g was added, depending on the sample being profiled. The change in penetration, 30 sec following the addition of the second load, was taken as the experimental penetration distance.

The materials studied were commercial formulations and included: EPR(I) and EPR(II), two ethylene-propylene rubber formulations used in making O-rings; Viton®, a copolymer of vinylidene fluoride and hexafluoropropylene used for O-rings; cross-linked polyethylene, a chemically cross-linked material used as a cable insulation; PE, a noncross-linked medium-density polyethylene used as cable insulation; polyurethane, a flexible urethane used as a cable

insulation; Tefzel®, a copolymer of ethylene and tetrafluoroethylene used as cable insulation; chlorosulfonated polyethylene (Hypalon®), a formulation used for cable jacketing; chloroprene (Neoprene®), a formulation used for cable jacketing; CLPO (cross-linked polyolefin), a copolymer of ethylene and ethyl vinyl acetate used for cable insulation; and PVC (polyvinyl chloride) a formulation used for cable jacketing.

DISCUSSION OF OXYGEN PENETRATION EFFECTS

The rate at which many common polymer materials can attain equilibrium oxygen saturation can be quite high. The time required for sorption of one half of the equilibrium oxygen content in a planar sheet of material having thickness l is given[21] by Equation 1 (D is the diffusion coefficient).

$$t_{1/2} = .04919 \frac{l^2}{D} \qquad (1)$$

Many polymers have D values in the approximate range of 10^{-6} to 10^{-7} cm^2/sec.[22] Thus, polymers of several millimeters thickness have $t_{1/2}$ in the range of minutes to hours, so that such materials achieve equilibrium saturation of air shortly after being molded.

If an air-saturated polymer sample is placed in a radiation environment, homogeneous oxidation will take place initially. At sufficiently high oxidation rates--depending on dose rate, radiation yield [$G(-O_2)$], oxygen permeation rate, and specimen thickness--the initially dissolved oxygen may be used up faster than it is replenished from the atmosphere. This gives rise to heterogeneous degradation with the oxidation rate in interior regions of the material decreasing to zero (or in some cases to some fixed rate lower than that near the surfaces). For materials and radiation conditions which result in heterogeneous degradation, an indication of the absorbed dose by which strongly heterogeneous degradation is already taking place may be obtained by calculating the equivalent dose required to use up the oxygen initially dissolved in the material. We obtain the following expression for this dose, R, in rads:

$$R = \frac{S \cdot P}{(1.03 \times 10^{-2}) \cdot G(-O_2)} \qquad (2)$$

where S is oxygen solubility in mol/g·atm, and P is the oxygen pressure in atm. $G(-O_2)$ is molecular yield per 100 eV absorbed energy. Table 1 gives solubility data and reported $G(-O_2)$ yields for several common polymer types, together with the calculated values for the equivalent dose required to cause reaction of the amount of oxygen initially dissolved in a specimen equilibrated in air at an assumed oxygen pressure of .2 atm. From the data in the table, it can be seen that the transition from homogeneous to strongly heterogeneous degradation of these polymers will occur at quite low doses--generally less than a few tenths of a megarad.* For virtually all polymers, measurable degradation occurs only after substantially higher doses. Thus, where oxidation inhomogeneities occur, the degradation can typically be treated as coming entirely from a heterogeneous mechanism.

If the oxygen permeation constant, P, and the yield of oxygen consumption, $G(-O_2)$, for the material remain relatively constant as a function of total absorbed dose, a steady state in heterogeneous oxidation will be approached. If the rate of oxygen consumption by reaction with free radicals generated by the radiation exceeds the rate of supply of oxygen from the edges of the polymer sample, distinct regions of oxidized and nonoxidized polymer can result.

In comparing polymer samples irradiated at different dose rates, those exposed at the highest dose rate may degrade heterogeneously, becoming oxidized only near the surfaces. At successively lower dose rates, oxidation depth will become progressively larger. Eventually, at sufficiently low dose rates, the oxygen can fully penetrate the sample, giving rise to oxidation which is homogeneous throughout the material.

OBSERVATION OF HETEROGENEOUS OXIDATION: EPR

As a polymeric material degrades, its physical and mechanical properties can undergo changes due to crosslinking, scission, plasticizer loss, or changes in morphology. The cross-sectional polishing technique for optical identification of heterogeneous degradation is indirectly based on such changes. Areas of the polymer having sufficiently different physical properties take on different lusters upon polishing. When examined under an optical microscope, with the sample positioned at an angle such that the light from a strong light source is reflected into the microscope lens, areas of the sample that have experienced

*Note that certain fluorocarbons are exceedingly susceptible to radiation degradation and may be an exception to this.

TABLE 1

Literature Values for Solubility and $G(-O_2)$ Yields, and Calculated Equivalent Dose Required to Cause Reaction of Dissolved Oxygen in Equilibrium With Air (.2 Atm O_2 pressure)

Polymer	S^* (ref)	$G(-O_2)$ (ref)	Equivalent Dose (Mrad)
PE	2.2×10^{-6} (18)	10 (23) 22 (24)	.04 .02
PVC	7.5×10^{-6} (22)	12 (25) 30 (25) 57 (26)	.15 .05 .03
EPR	5.4×10^{-6} (22)	20 (27) 40 (27) 60 (27)	.05 .03 .02
CLPO	3.1×10^{-6} (22)	10 (28)	.06

* Expressed in mol/g·atm

significantly different degradation show up as bands having different reflectivity. Additionally, in some materials, a slight color difference can be seen between regions having differences in oxidation. We have successfully applied this technique to the observation of heterogeneous oxidation degradation in a variety of different material types.[29*]

In a related technique described in a preliminary communication, we have examined relative changes in material hardness across the surface of a cross-sectioned, polished sample.[29] This technique is more quantitative, and allows a detailed determination of the degradation profile in terms of changes in physical properties. Our earlier profiles were obtained using a Knoop microhardness tester, which is most appropriate for harder polymers.[29,30] Determinations of changes in relative hardness across cross-sectioned samples referred to in this report use a somewhat different experimental technique. Data in the figures are given in terms of changes in penetration distance of a tiny, specially built, weighted probe into a sample; no effort was made to correlate penetration distances with standard hardness units as defined by any of the arbitrarily set scales used in the many hardness penetration tests which have been described.[30] A smaller penetration indicates an increase in material hardness; larger penetration indicates a decrease in material hardness. Penetration under load can be related to changes in material modulus: decreased penetration corresponds to higher modulus; increased penetration corresponds to lower modulus. Exact relationships depend on experimental procedures and probe tip geometry.[31]

In an additional technique employed, the densities of pieces of degraded samples are determined using a salt gradient column.[12] This technique provides a profile on

*Polished samples were also examined using a scanning electron microscope, and in some cases bands could be seen in the surface texture; however, the simple optical microscope was generally much more successful. We have also performed experiments which indicate that optical evaluation following cross-sectional polishing may be of some value as a more quantitative technique, giving information on oxidation profile shape as well as indicating the depth of significant oxidation. We have scanned the cross-sectional surface of the samples with a finely focused laser beam, and measured the relative amount of reflected light as a function of position. The laser measurements indicate a strong heterogeneity which corresponds to the visible ring, but show a gradient in reflectivity rather than two single regions as seen by the eye.

oxygen uptake in the sample--information which is complementary to that provided by the techniques based on changes in mechanical properties. Oxidation of samples normally leads to increases in sample density.

The photos in Figure 1 were obtained for a series of EPR(I) samples, cut from a square sheet of gasket material, which were irradiated and then cross sectioned and polished. Strongly heterogeneous degradation is indicated for the samples irradiated in air at the highest dose rate by the appearance of distinct optical bands (rings). Thus, rings are clearly observable for samples B and C. These samples were irradiated at 6.7×10^5 rad/h to 165 Mrad and 297 Mrad, respectively. In contrast, samples A, D, and E do not exhibit oxidative rings. A is an unirradiated sample, D was irradiated at a lower dose rate (1.1×10^5 rad/h to 175 Mrad), while E was irradiated under inert atmosphere.

Figure 2A shows probe penetration profiles indicating changes in relative hardness on cross-sectioned samples of the EPR material of Figure 1. For unirradiated material, the profile is essentially flat (solid squares). For the samples irradiated at 6.7×10^5 rad/h to a dose of 297 Mrad, a distinct flat-bottomed, U-shaped profile is seen (open circles). The boundary position between optical bands (photo C, Figure 1) corresponds to the steep part of the profile (slightly less than 20 percent of the way in on both sides). The irradiated material has become significantly harder (i.e., increased modulus) with the largest increase occurring at the interior portion where oxygen is absent. Figure 2B shows data for an EPR sample irradiated at 6.7×10^5 rad/h to a lower total dose (165 Mrad). A somewhat more shallow profile is obtained, but with no significant change in the oxygen penetration distance (squares). For a sample irradiated at a lower dose rate (1.1×10^5 rad/h to 175 Mrad) the profile approaches a homogeneous condition, showing only a slight, shallow curvature (Figure 2B, triangles).

Figure 3A shows density gradient data for EPR samples B and C of Figure 1, which were irradiated at 6.7×10^5 rad/h. Areas of high and low oxidation seen by density gradient measurements show an excellent correlation to the bands of different optical reflectivity observed for these samples. Again, relatively distinct oxidized and nonoxidized regions are indicated. The boundary position between optical bands correlates well with the position of rapid change in the curve generated using the density gradient column.

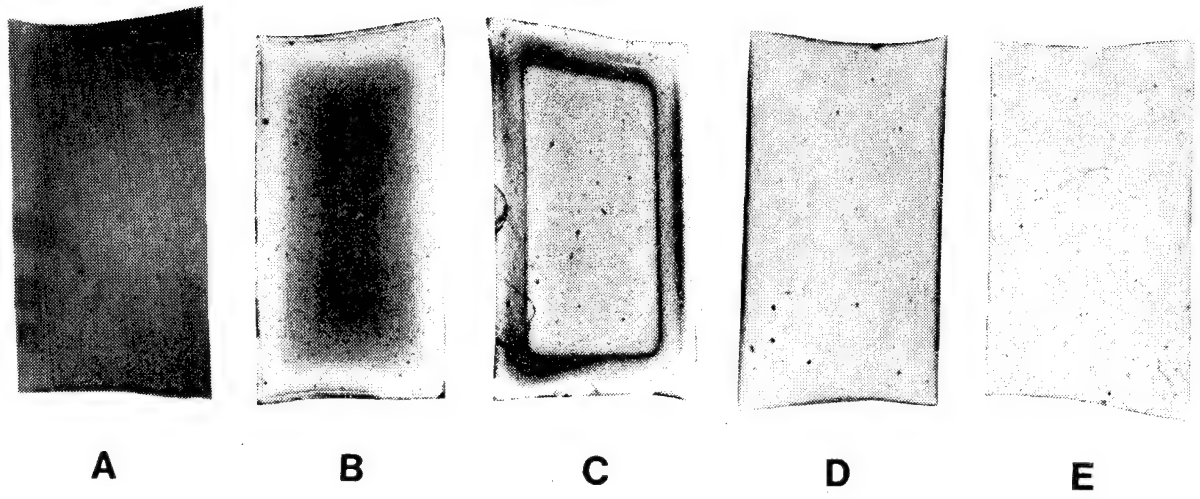

Figure 1. Cross-sectioned, polished samples of gamma irradiated EPR.
A: Unirradiated material.
B: 6.7×10^5 rad/h (in air) to 165 Mrad.
C: 6.7×10^5 rad/h (in air) to 297 Mrad.
D: 1.1×10^5 rad/h (in air) to 175 Mrad.
E: 1.1×10^6 rad/h (in vacuum) to 253 Mrad.
All irradiations carried out at 70°C. Actual sample thickness = 3.15 mm.

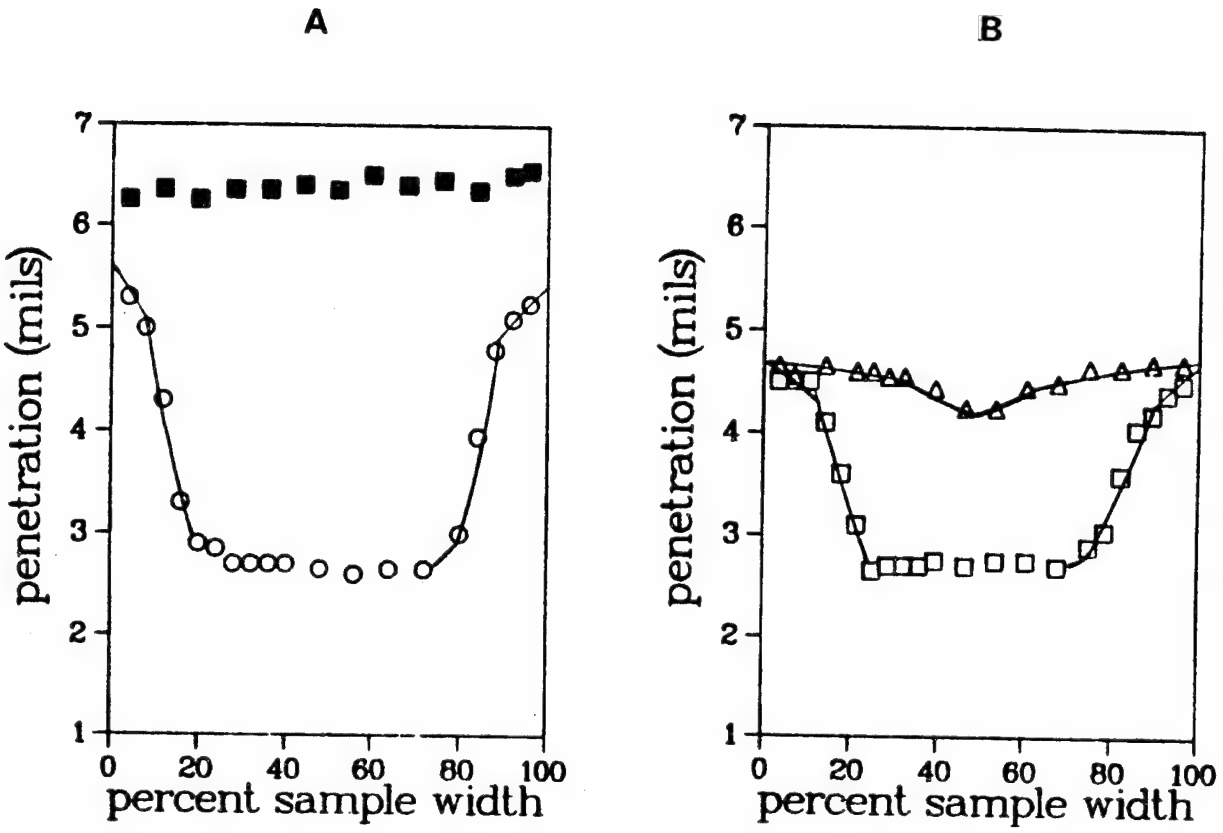

Figure 2. Profiles of relative hardness in terms of penetration distance of a weighted probe into cross-sectioned samples of irradiated EPR.
A: ■ = unirradiated material,
○ = 6.7 x 10^5 rad/h to 297 Mrad,
B: □ = 6.7 x 10^5 rad/h to 165 Mrad,
△ = 1.1 x 10^5 rad/h to 175 Mrad.
Experimental load was 5 g.

Figure 3B compares density data on two samples (B and D of Figure 1) that were irradiated to similar dose, but at different dose rates. Strongly heterogeneous oxidation is indicated for the high-dose-rate sample, in contrast to nearly homogeneous oxidation for the low-dose-rate sample. This is again in accord with conclusions reached by optical examination of polished samples. Comparison of Figures 2 and 3 shows the excellent correlation between the relative hardness and density profile results.

As might be expected, the optical rings became progressively fainter on going to lower doses; rings were not visible at doses below about 50 Mrad. However, the size of the rings in this material did not change significantly as a function of dose at constant dose rate. Similarly, relative hardness and density gradient experiments indicate that while the profiles obtained become more shallow at lower total doses, the oxidation depth has little dose dependence. These observations indicate that oxygen permeation and consumption rates in this material are not significantly dependent on dose.

Further experiments were performed on the EPR material irradiated to 297 Mrad total dose at 6.7×10^5 rad h. This sample was sectioned into areas corresponding to oxidized and nonoxidized regions as indicated by the rings (photo B, Figure 1). The oxidized (outer) region and unoxidized (inner) region were extracted with THF. The swelling ratios were 80 percent for the outer region and 47 percent for the inner region; corresponding inner and outer regions of an unirradiated sample gave swelling ratios of 108 percent and 107 percent. These data indicate substantial differences in the relative ratios of cross-linking and scission in the regions corresponding to the interior and exterior portions of the sample, with relatively much higher cross-linking in the unoxidized regions. These results are also consistent with the modulus increases noted from the profiles of relative hardness.

OXIDATION DEPTH AND OXIDATION PROFILES

Some further discussion of oxidation gradient shapes is useful at this point. The visual rings seen in cross-sectioned, polished samples correspond to areas having large differences in the extent of oxidation, and as such are useful for identification of heterogeneous degradation and for a qualitative or semiquantitative determination of the depth of significant oxidation. However, the exact shape of the degradation profile will depend on the details of the under-

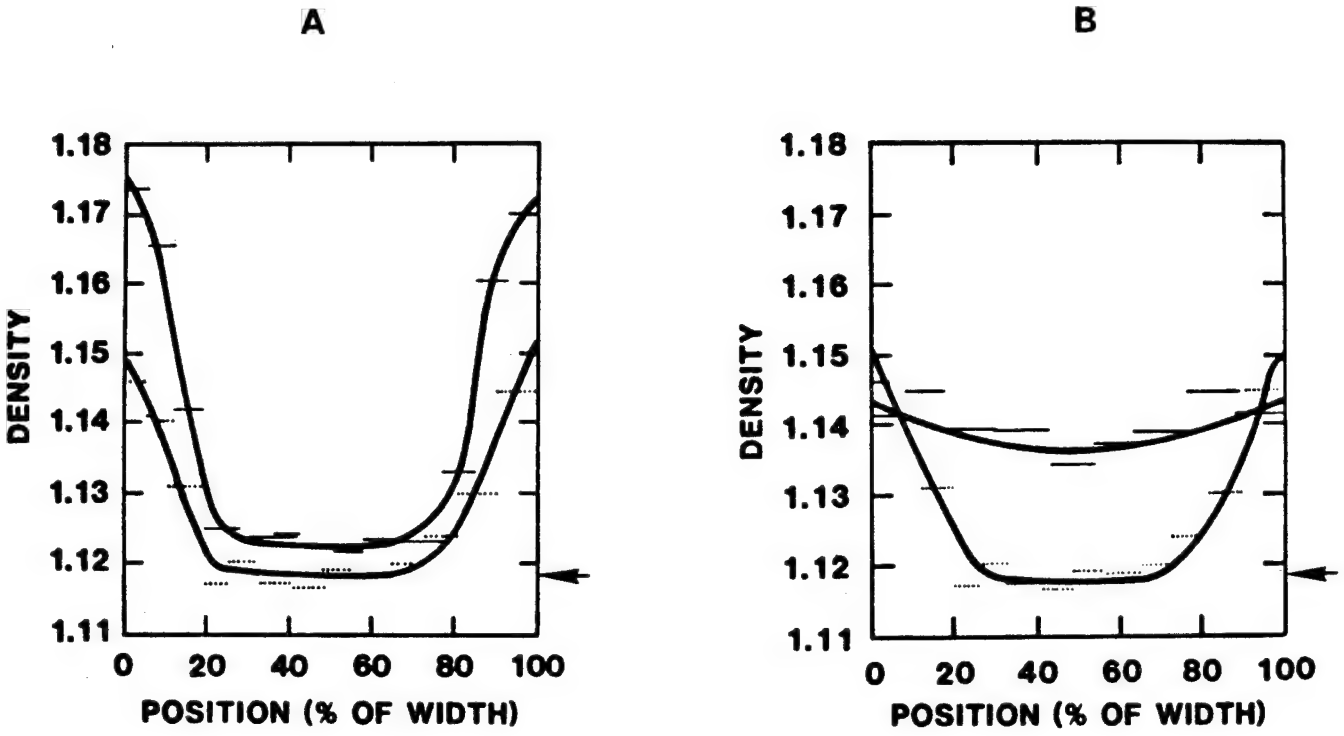

Figure 3. Density profiles for irradiated EPR samples.
A: EPR samples irradiated in air at 6.7 x 10^5 rad/h, 70°C. Solid line symbols (upper curve) are for 297 Mrad absorbed dose. Dotted line symbols (lower curve) are for 165 Mrad absorbed dose.
B: EPR samples irradiated in air at 70°C to similar total dose, but at different dose rates. Dotted line symbols are for 165 Mrad at 6.7 x 10^5 rad/h. Solid line symbols are for 175 Mrad at 1.1 x 10^5 rad/h. The arrow in both A and B shows the density of unirradiated material, which gives a flat profile.

lying oxidation kinetics. For instance, Cunliffe and Davis[32] assumed that the oxidation kinetics for photo-oxidation can be described by a free radical mechanism similar to that proposed by Boland[33,34] and Bateman[35] for the thermal oxidation of hydrocarbons in the liquid phase. Depending upon the relative importance of propagation and termination reactions, they predicted oxidation profiles ranging from gentle parabolic-like shapes to step-like transitions. Thus oxidative rings visible from cross-sectional polishing may represent situations ranging from step transitions between oxidized and nonoxidized regions, to more gradual transitions between heavily oxidized regions and regions having either no oxidation or light oxidation. The term oxidation depth has quantitative meaning in the former limit, but has a somewhat more qualitative meaning in the latter.

Ideally, it should be possible to calculate the depth and shape of oxidative penetration for a given material under a particular set of circumstances. Equations for treating the problem of gradients in systems having simultaneous diffusion and reaction have been described.[36-39] The problem is quite complex; moreover, a solution would require knowledge of many parameters for a particular system, such as oxygen solubility and diffusion coefficient, and oxygen uptake yield, $G(-O_2)$. To eliminate diffusion effects in the determination of $G(-O_2)$, experiments would need to be carried out on a powder or thin film, and it would be difficult to guarantee that such a sample would be identical, with respect to parameters such as morphology, compared to a molded polymeric material of interest. Moreover, $G(-O_2)$ may be different at different dose rates due to mechanistic reasons other than diffusion. Also, as mentioned before, the shape of the gradient will depend heavily upon the details of the kinetics for the chemical reactions involving oxygen.[32] A determination of such kinetic details in a given material would be a difficult task. In general, it would seem much easier to identify heterogeneous degradation directly using the techniques described in this paper, than to perform the experiments and calculations necessary to compute profile shapes.

HETEROGENEOUS DEGRADATION AND MACROSCOPIC PROPERTIES: VITON® DEGRADATION

To illustrate how dramatic the differences in degradation can be at different oxidation penetration levels, we now present an extensive set of tensile data which were obtained on a Viton® material. For this material, degradation

behaviors are so different that the mechanical properties actually appear to degrade in opposite directions at high and low dose rates. Thus, at the highest dose rate of 5.5×10^5 rad/h (Figure 4, circles), the elongation drops rapidly while the tensile strength decreases only slightly. The high-dose-rate degraded sample becomes hard and brittle. In contrast, at the lowest dose rate of 1.3×10^4 rad/h (Figure 4, squares), the elongation remains very high while the tensile strength drops rapidly. The low-dose-rate degraded sample becomes soft and is extremely rubbery and easily stretched.

Figure 5 shows a series of solvent-swelling experiments performed both on the samples irradiated at the highest (5.5×10^5 rad/h) and lowest (1.3×10^4 rad/h) dose rates. The data indicate a major difference in the degradation modes at the different dose rates: at 5.5×10^5 rad/h, the sample undergoes predominantly cross-linking; at 1.3×10^4 rad/h the sample suffers extensive net scission.

These degradation differences can be understood in terms of large differences in oxidative degradation depth over this range of dose rates. Table 2 presents data on oxidative penetration depth, as determined by optical examination of cross-sectioned, polished samples, for the Viton® material irradiated over the dose-rate range for which tensile data is shown in Figure 4. Strongly heterogeneous degradation, with oxidation only near the edges, is seen at the highest dose rate. At the lowest dose rate, the results indicate that the degradation approaches homogeneous oxidation throughout.

Figure 6 shows data for cross-sectional profiling of relative hardness on Viton® samples irradiated in the dose-rate range of interest. The results are in good agreement with conclusions reached by optical examination. Strongly heterogeneous degradation is found at the highest dose rate of 5.5×10^5 rad/h (open squares, Figure 6); here, an oxidized region extends just slightly more than 15 percent of the way in from either side of the sample. Again, at successively lower dose rates, evidence of progressively deeper oxidation is found: data for material irradiated at 1.8×10^5 rad/h, where degradation extends just over 20 percent of the way in, is given as circled crosses. Samples irradiated at still lower dose rate were too soft and tacky to test.

Relative hardness data on unaged Viton® is also given in Figure 6: this is the flat profile which is indicated by solid squares. Comparison of this profile with profiles of

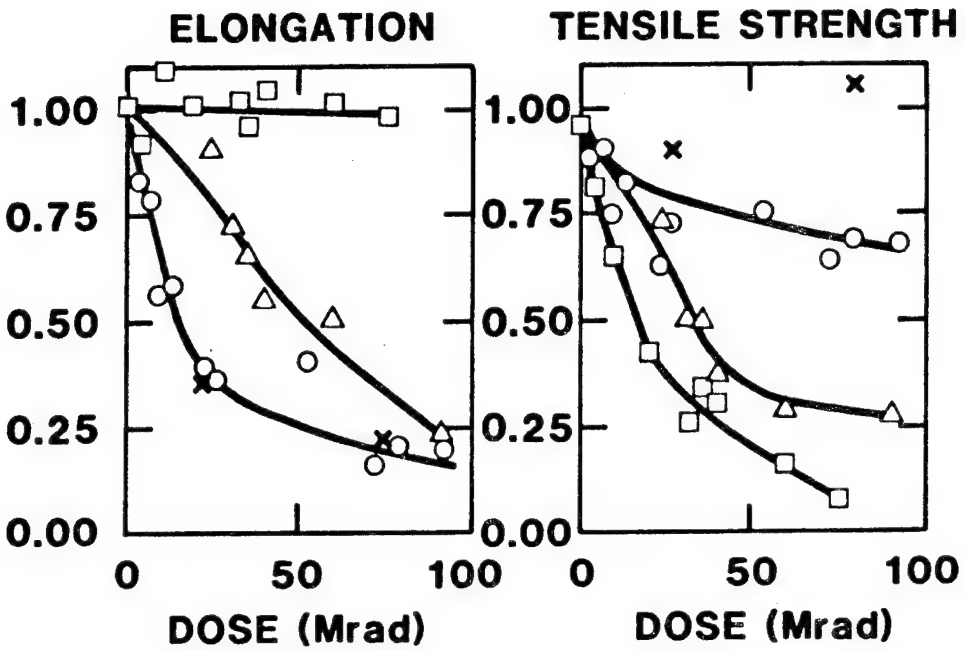

Figure 4. Change in ultimate tensile properties for a Viton® material irradiated at 70°C using three different dose rates.
○ = 5.5 x 10^5 rad/h (in air),
△ = 9.2 x 10^4 rad/h (in air),
□ = 1.3 x 10^4 rad/h (in air),
X = 5.5 x 10^5 rad/h (in inert atmosphere).
Left: reduced elongation (e/e_o),
Right: reduced tensile strength (T/T_o).

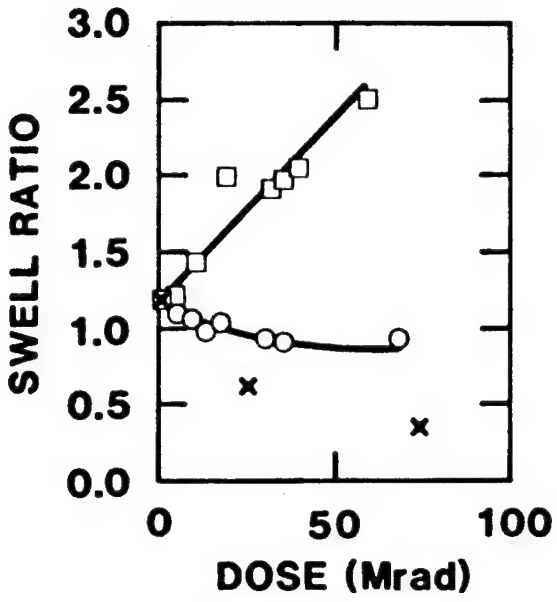

Figure 5. Solvent swelling data for the Viton® material of Figure 4 (symbols have same meaning). Solvent was THF. Data calculated as: (swelled weight minus dry weight) divided by dry weight.

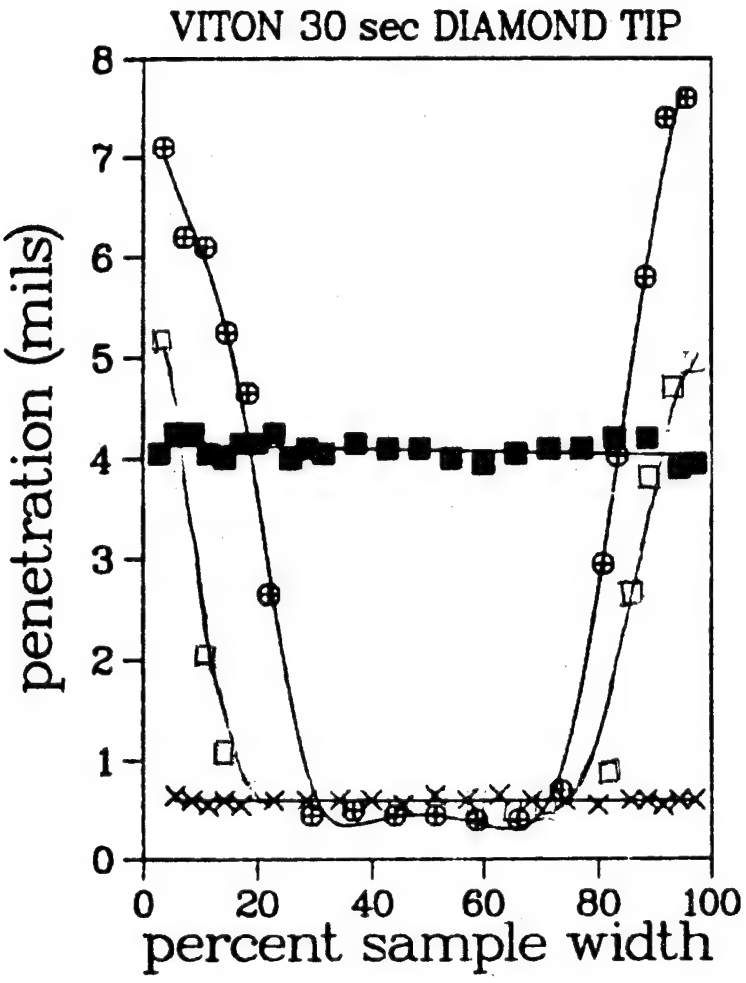

Figure 6. Hardness profiles for irradiated Viton® samples.
■ = unirradiated material,
□ = 5.5 x 10^5 rad/h to 178 Mrad,
⊕ = 1.8 x 10^5 rad/h to 186 Mrad,
X = 9.0 x 10^5 rad/h to 191 Mrad (under vacuum).
Experimental load was 3 g.

TABLE 2

Oxidation Depth as Determined by Cross-Sectional Polishing of Viton® Material Irradiated at 70°C, Using Different Dose Rates*

Dose Rate (rad/h)	Oxidation Depth**	Oxidation as % of Total Thickness
5.5×10^5	.33 mm	35%
1.8×10^5	.42 mm	44%
9.2×10^4	.78 mm	82%
1.3×10^4	complete	100%

* Ring size was relatively dose-independent

** Sample Thickness = 1.91 mm

the degraded samples demonstrates opposite degradation trends in oxidized and nonoxidized regions of the sample. Near the edges, under conditions of strong oxidation, the material becomes softer as it degrades. In the interior, the sample becomes relatively harder as it degrades.

All of the results obtained on Viton® samples irradiated in air at different dose rates (tensile property trends, optical rings, relative hardness profiles, and solvent swelling) comprise a consistent picture of differences in degradation mechanism resulting from oxygen-diffusion-limited effects. The samples irradiated at high dose rate, for which a large portion of the interior is oxygen starved, degrade predominantly by cross-linking, becoming harder. The samples irradiated at low dose rate, for which oxidation occurs throughout the material, degrade predominantly by chain scission, becoming softer.

Tensile and swelling data for Viton® samples irradiated under vacuum where nonoxidative degradation proceeds throughout (shown as crosses in Figures 4 and 5), further underscore these trends. Thus, for the vacuum-irradiated samples, elongation drops rapidly (similar to the samples irradiated at high dose rate in air), while tensile strength decreases even less than for the high-dose-rate irradiated samples. The result is that the vacuum-irradiated material becomes even more strongly and rapidly embrittled than in the case of high-dose-rate irradiation in air. Similarly, the total cross-link density, as determined by solvent swelling, increases in the case of vacuum-irradiated samples (as seen by the large drop in swelling ratio). This increase is even more pronounced compared with the samples irradiated at high dose rate in air.

Data indicating relative hardness changes for a Viton® sample irradiated under vacuum are also presented in Figure 6. This flat profile, indicated by crosses, corresponds well to the hardened interior (anaerobic) regions of samples irradiated at high dose rates in air. Clearly, for Viton®, the effect of oxygen on degradation-induced mechanical property changes is extremely large.

COMPILATION OF HETEROGENEOUS DEGRADATION DATA

Table 3 summarizes our data on the depth of the oxidized regions in a series of commercial polymer materials irradiated at several different dose rates and temperatures. The data are useful as general indicators for the extent of oxidative penetration to be expected for bulk samples of common

polymers as a function of dose rate in air. However, the values given are by no means absolute numbers for a given polymer type. Different $G(-O_2)$ values are to be expected for different commercial samples of the same polymer type, depending upon morphology and upon additives (particularly antioxidants). Permeation constants will also vary somewhat again dependent upon both morphology and additives (such as plasticizer).

The data in Table 3 show some general correlation between oxidative penetration and literature values for oxygen permeation. For instance, the ethylene-tetrafluoroethylene copolymer (Tefzel®) has the lowest permeation constant of any polymer in the table, and also has the smallest oxidation region. EPR has the highest permeation constant in the table and the EPR materials have the highest oxidation penetrations. A significant temperature dependence for oxidative penetration is also seen in the data, with increased penetration at increased temperature.

In an effort to provide further confirmation of the connection between oxidative degradation and the appearance of rings, a number of the materials were irradiated using doses and dose rates similar to those of Table 3, but under inert atmosphere; in no case did rings appear. Conditions for samples irradiated in the absence of oxygen are summarized in Table 4.

For most of the materials which we have examined, oxidative penetration depth did not change significantly as a function of absorbed dose at constant dose rate. We did identify a few cases where at a constant dose rate, the region of maximum oxidation (in terms of the optical rings), became smaller at higher total dose. The most striking example was for a PVC material irradiated at 2.9×10^4 rad/h and 43°C. Oxidative ring size in this material as a function of absorbed dose is shown in Table 5. We believe that the change in ring size in this material results from an increased oxidation rate at longer times (i.e., higher doses), due to the thermally induced breakdown of peroxides formed during irradiation. This breakdown of peroxides would result in the formation of additional free radicals to compete for oxygen with radicals formed directly from the primary radiation processes. The importance of this mechanism in the radiation oxidation of this same PVC material has been documented in an earlier paper.[10]

It is interesting to note one result of such a mechanism giving decreased oxidative penetration at high doses (long times). If a series of samples all aged to similar high dose

TABLE 3 Oxidative Degradation Depth (as Indicated by Ring Size) of Some Common Polymer Materials as a Function of Dose Rate and Temperature

Material Type	Irradiation Temperature	Literature Oxygen Permeation Constant* and (Temp., ref.)	Material Thickness	Oxidative Penetration Depth Dose Rate and (Dose)			
EPR(I)	70°C	19.0 (25°C, 22)	3.15 mm	.54 mm 6.7×10^5 rad/h (165 Mrad)	no rings 1.1×10^5 rad/h (121 Mrad)		
EPR(II)	70°C	19.0 (25°C, 22)	1.91	.56 mm 6.7×10^5 rad/h (226 Mrad)	no rings 1.1×10^5 rad/h (143 Mrad)		
	ambient				.88 mm 1.1×10^5 rad/h (114 Mrad)		
Viton®	70°C	2.2 (26°C, 40)	1.91 mm	.33 mm 5.5×10^5 rad/h (178 Mrad)	.42 mm 1.8×10^5 rad/h (186 Mrad)	.78 mm 9.2×10^4 rad/h (130 Mrad)	no rings 1.3×10^4 rad/h (76 Mrad)
	43°C					.16 mm 9.6×10^4 rad/h (144 Mrad)	
Crosslinked PE	43°C	---	.75 mm	.15 mm 8.9×10^5 rad/h (119 Mrad)	.35 mm 6.4×10^4 rad/h (116 Mrad)	no rings 1.7×10^4 rad/h (114 Mrad)	
Med. Density PE	60°C	5.5 (30°C, 41)**	.68 mm	.17 mm 3.1×10^5 rad/h (52 Mrad)	no rings 2.4×10^4 rad/h (57 Mrad)		
	43°C			.09 mm 9.5×10^5 rad/h (135 Mrad)	.25 mm 6.0×10^4 rad/h (51 Mrad)	no rings 2.0×10^4 rad/h (26 Mrad)	

TABLE 3 Continued

Polyurethane	70°C	---	2.01 mm	.30 mm 7.2 x 10^5 rad/h (156 Mrad)			
Tefzel®	70°C	0.6 (25°C, 42)	.28 mm	.08 mm 5.7 x 10^5 rad/h (27 Mrad)	no rings 9.3 x 10^4 rad/h (16 Mrad)		
	43°C				.12 mm 1.0 x 10^5 rad/h (46 Mrad)		
Chlorosulfonated PE	(ambient)***	3.3 (30°C, 40)	1.21 mm	.13 mm 9.6 x 10^5 rad/h (162 Mrad)	.27 mm 4.9 x 10^4 rad/h (134 Mrad)		
Chloroprene	(ambient)***	4.0 (25°C, 40)	1.86 mm	.17 mm 9.1 x 10^5 rad/h (159 Mrad)	.22 mm 4.9 x 10^4 rad/h (135 Mrad)	.34 mm 4.7 x 10^4 rad/h (129 Mrad)	.72 mm 8.4 x 10^3 rad/h (149 Mrad)
CLPO	(ambient)***		.75 mm	.06 mm 1.2 x 10^6 rad/h (175 Mrad)	.17 mm 2.2 x 10^5 rad/h (148 Mrad)	.22 mm 5.2 x 10^4 rad/h (141 Mrad)	
PVC	43°C	1.0 (25°C, 40)****	1.43 mm	.12 mm 9.4 x 10^5 rad/h (223 Mrad)			

* Units of $\frac{\text{(std cc) (cm thickness)}}{\text{(sec) (sq cm area) (cm Hg pressure drop)}} \times 10^{10}$

** density = .922

*** ambient temperature of the source: 10^6 rad/h was approximately 42°C. 10^5 rad/h was approximately 28°C, 10^4 rad/h was approximately 25°C.

**** 20% plasticizer (DOP)

TABLE 4

Conditions for Materials Irradiated Under Inert Atmosphere
Using Radiation Doses and Dose Rates Similar to Those of Table 3

Material	Dose Rate (rad/h)	Temp (°C)	Dose (Mrad)
EPR-A	1.1×10^6	70	253
Viton®	1.0×10^6	70	191
PE	9.2×10^5	43	216
PE	7.1×10^4	43	196
Tefzel®	1.0×10^6	70	22
Neoprene®	1.0×10^6	43	100
Crosslinked Polyethylene	1.1×10^6	43	103

TABLE 5

Oxidative Penetration Distance in PVC Material Irradiated at 2.9×10^4 rad/h as a Function of Total Dose*

Dose (Mrad)	24.6	34.4	43.7	58.7
Oxidative Penetration Distance	full** penetration	.54 mm	.45 mm	.30 mm

* Irradiation temperature = 43°C

** Sample Thickness = 1.43 mm

but at different dose rate are compared, the oxidative penetration depth on going to progressively lower dose rates could appear to increase at first (oxygen-diffusion dominance), but then level off or even decrease at dose rates sufficiently low as to give long enough experimental time periods for appreciable thermal peroxide breakdown to occur.

We have also observed a few cases where the oxidative ring size was different at different surfaces of the same material. Such differences apparently reflect inhomogeneities in material composition such as morphology or the concentration of formulation components or impurities.

In examining samples by cross-sectional polishing, it should be noted that while the appearance of rings in oxidized samples is useful as a measure of heterogeneous oxidation, the absence of rings in a sample is not conclusive proof of homogeneous degradation. For samples irradiated to low doses such that only modest physical changes have taken place, rings may not be visible. Also, at dose rates where oxygen is reaching the center of the material, but in a depleted concentration such that homogeneity is not quite attained, a slight oxidative inhomogeneity with a broad, very shallow parabolic shape may remain. This slight heterogeneity may not show up using the polishing technique.

IMPLICATIONS FOR ACCELERATED AGING EXPERIMENTS

This report has focused on studies of oxidative heterogeneities in irradiated polymers, and has pointed out that this can be an important factor leading to significant differences in the macroscopic property changes resulting from absorption of equivalent radiation dose at different dose rates. In extreme cases, as with Viton®, a material may degrade in completely different ways under conditions leading to different oxidative penetration depths. This is because very different degradation mechanisms can occur in the presence or absence of oxygen.

The occurrence of strongly heterogeneous oxidation in samples irradiated at high dose rates is an important consideration in the design of accelerated aging experiments. For accelerated aging experiments using very high dose rates, degradation in the interior regions of materials may take place under anaerobic conditions. When this occurs, such high dose-rate exposures generally cannot be expected to yield predictive information on degradation behavior or degradation rate in long-term application environments having low radiation levels, where oxidation proceeds throughout the

sample. Circumventing this problem may require finding conditions of sufficiently low dose rate, for accelerated tests, that homogeneous oxidation is approached.

One general concept often used in conjunction with accelerated testing is that of "overstress". In the case of radiation aging tests, materials may be subjected to a short-term radiation exposure using both a dose rate and total dose that are many times higher than those expected during the useful lifetime of the material in the intended application environment.[43] The idea is to use an excess total dose in the accelerated test that will compensate for the fact that some differences in degradation due to dose rate may occur (i.e., higher damage at equivalent dose may be found). The assumption is that if the material retains enough of its essential properties to perform a particular function after the accelerated test, the same should hold true after long-term exposure in the application environment. However, the Viton® data demonstrate why this approach can be invalid. Because of differences in degradation mechanism which result from oxygen diffusion effects at different dose rates, the fundamental degradation modes and resulting material property changes in this material are essentially opposite at high and low dose rates (embrittlement at high dose rates, softening at low dose rates). Failure modes and failure criteria should also be very different for the samples irradiated at the different dose rates. Given the opposite trends in degradation effects, the overstress approach cannot compensate for the effects of dose rate. In fact, use of an overdose will actually achieve the opposite of the intended effect, with progressively higher dose moving the material properties progressively further away from the properties which result at lower dose rate.

In comparing results of radiation degradation at different dose rates, it should be noted that diffusion-limited oxidation is not the only factor that can lead to apparent dose-rate effects in the presence of oxygen. Other chemical mechanisms can also give rise to such effects.[10,12,27,44] Thus, the occurrence of homogeneous oxidation over a given range of dose rates does not necessarily imply that no dose-rate effect will be observed over that range. Two such chemical mechanisms which can cause dose-rate effects are discussed by us in both previous[10,12] and forthcoming[45] reports. Complete understanding of the differences in radiation-induced degradation behavior of materials under different dose rates, which is a prerequisite for design and interpretation of accelerated aging experiments, requires the sorting out of the various mechanisms that can lead to dose-rate effects in a given material.

SUMMARY AND CONCLUSIONS

This report describes the application of useful techniques for the rapid identification of oxidative inhomogeneities in degraded polymeric materials. For cross-sectional evaluation, samples are mounted and polished using standard diamond polishing wheels available in a metallographic laboratory. Areas of the material having different extents of degradation are seen as bands of varying reflectivity when examined microscopically using a strong point source of light. The differences in surface luster after polishing result from differences in the material's physical properties as a function of degradation. Further information on gradient shapes, with respect to physical properties, may be obtained by profiling relative material hardness (in terms of penetration of a weighted probe) across the cross-sectional surface. Additional useful information on gradients in oxygen uptake may be obtained using density gradient columns. These techniques, together with solvent extraction experiments on cut-up samples, give consistent results with respect to the extent of oxidative penetration in degraded polymers.

Examples have been shown of polished samples of several different commercial polymer materials irradiated at varying dose rates. The range of dose rates over which significant oxidation gradients occur can be substantially different in different materials. This will be a complicated function not only of thickness, but also of oxygen permeation rate and oxygen consumption rate, $G(-O_2)$, for a given material. We find that for many common polymer materials, oxidation depths of fractions of millimeters are common over a dose-rate range of 10^4-10^6 rads/h in the presence of air. As expected, oxidation is seen to proceed progressively deeper into the sample as the dose rate is lowered. We have calculated that the onset of strongly heterogeneous degradation will occur at very low total doses for common materials (on the order of a fraction of a Megarad), as initially dissolved oxygen is used up. We have observed that in many cases, the size of the oxidized area in the polymer remains essentially constant as a function of total dose, indicating that both $G(-O_2)$ and permeability are often little changed as a function of degradation. One case of decreasing oxidative penetration distance as a function of dose was described, which was associated with increasing $G(-O_2)$.

Strong differences in degradation are seen to occur due to differences in oxidative penetration depth which result

under different radiation conditions. A striking example occurs with Viton®. In the absence of oxygen, the material becomes progressively more cross-linked and harder. In the presence of oxygen, the material undergoes scission, and becomes progressively softer. The result is that samples irradiated at high dose rate, where oxidation can be shown to occur only near the surface, exhibit trends in degradation behavior characteristic of samples irradiated under vacuum (i.e., becoming brittle). Samples irradiated at comparatively lower dose rates, where extensive oxygen permeation can be shown to occur, degrade in the opposite way (i.e., becoming soft and stretchable).

REFERENCES

1. A. Charlesby, Proc. Roy. Soc., A215, p 187 (1952).

2. D. Ballantine, G. Dienes, B. Manowitz, P. Ander, and R. Mesrobian, J. Polym. Sci., 13, p 410 (1954).

3. L. St. Pierre and H. Dewhurst, J. Chem. Phys., 29, p 241 (1958).

4. H. Matsuo and M. Dole, J. Phys. Chem., 63, p 837 (1959).

5. F. Makhlis, Radiation Physics and Chemistry of Polymers, (New York: Wiley, 1975), p 151.

6. A. Chapiro, Radiation Chemistry of Polymeric Systems, (New York: Interscience, 1963), p 361.

7. A. Sisman, W. Parkinson, and C. Bopp, in Radiation Effects on Organic Materials, R. Bold and J. Carroll, Eds., (New York: Academic, 1963), p 171.

8. W. Schnabel, in Aspects of Degradation and Stabilization of Polymers, H. H. G. Jellinek, Ed., (Amsterdam: Elsevier, 1978), p 169.

9. M. Dole, The Radiation Chemistry of Macromolecules, (New York: Academic, 1973), Ch. 13, p 263.

10. R. L. Clough and K. T. Gillen, J. Polym. Sci., Polym. Chem. Ed., 19, p 2041 (1981).

11. R. L. Clough and K. T. Gillen, Radiat. Phys. and Chem., 22, p 527 (1983).

12. K. T. Gillen and R. L. Clough, Radiat. Phys. and Chem., 22, p 537 (1983).

13. R. L. Clough and K. T. Gillen, Nucl. Technol., 59, p 344 (1982).

14. K. T. Gillen, R. L. Clough, and L. H. Jones, SAND81-2613, 1981.

15. R. L. Clough and K. T. Gillen, Radiat. Phys. Chem., 18, p 661 (1981).

16. K. T. Gillen and R. L. Clough, Radiat. Phys. and Chem., 18, p 679 (1981).

17. R. L. Clough, K. T. Gillen, J. L. Campan, G. Gaussens, H. Schonbacher, T. Seguchi, H. Wilski, and S. Machi, "Accelerated Aging Tests for Predicting Radiation Degradation of Organic Materials," to be published in Nuclear Safety.

18. T. Seguchi and K. Arakawa, JAERI M 9671, Japan Atomic Energy Research Institute (1981).

19. L. E. Samuels, Metallographic Polishing By Mechanical Methods, Second Edition, (New York: American Elsevier, 1971).

20. G. L. Kiel, Metallographic Laboratory Practice, Third Edition, (New York: McGraw-Hill, 1949).

21. J. Crank and G. Park, Diffusion in Polymers, (New York: Academic Press, 1969), p 16.

22. D. Mitchell, Sandia National Laboratories, unpublished data.

23. H. Matsuo and M. Dole, J. Phys. Chem., 63, p 837 (1959).

24. E. Lawton, R. Powell, and J. Balwit, J. Polym. Sci., 32, p 277 (1958).

25. E. Hegazy, T. Seguchi, and S. Machi, J. Appl. Polym. Sci., 26, p 2947 (1981).

26. C. Decker, J. Appl. Polym. Sci., 20, p 3321 (1976).

27. C. Decker, F. Mayo, and H. Richardson, J. Polym. Sci., A-1, 11, p 2879 (1973).

28. K. T. Gillen and R. L. Clough, unpublished data.

29. R. L. Clough and K. T. Gillen, "Techniques for Studying Heterogeneous Degradation in Polymers," to be presented at the 187th ACS National Meeting, St. Louis, April 8-13, 1984 (to be published in Polymer Preprints).

30. N. Bikales, Ed., Mechanical Properties of Polymers, (New York: Wiley, 1971).

31. K. T. Gillen, J. Appl. Polym. Sci., 22, p 1291 (1978).

32. A. V. Cunliffe and A. Davis, Polym. Deg. and Stab., 4, p 17 (1982).

33. J. L. Bolland, Trans. Far. Soc., 44, p 669 (1948).

34. J. L. Bolland, Rev. Chem. Soc., 3, p 1 (1949).

35. L. Bateman, Quant. Rev. Chem. Soc., 8, p 147 (1954).

36. J. Crank, The Mathematics of Diffusion, (London: Oxford, 1956).

37. R. C. Giberson, J. Phys. Chem., 66, p 463 (1962).

38. N. Billingham and T. Walker, J. Polym. Sci., Polym. Chem. Ed., 13, p 1209 (1975).

39. K. Ono, A. Kaeriyama, and K. Murakami, J. Polym. Sci., Polym. Chem. Ed., 13, p 2615 (1975).

40. S. Hwang, C. Choi, and K. Kammermeyer, Separation Science, 9, p 461 (1974).

41. C. Rogers, in Engineering Design for Plastics, E. Baer, Ed., (New York: Rheinhold, 1964), Ch. 9, p 609.

42. Tefzel Design Handbook, E. I. du Pont (Delaware: de Nemours & Co., 1973), p 22.

43. IEEE Std. (323-1974), Institute of Electrical and Electronics Engineers, 1974.

44. K. Arakawa, T. Seguchi, Y. Watanabe, N. Hayakawa, I. Kuriyama, and S. Machi, J. Polym. Sci., Polym. Chem. Ed., 19, p 2123 (1981).

45. K. T. Gillen and R. L. Clough, "Extrapolation Model for Combined-Environment Accelerated Aging Experiments," to be submitted to J. Polym. Sci.

DISTRIBUTION:

U.S. NRC Distribution Contractor
7300 Pearl Street
Bethesda, MD 20014
375 copies for RV

Ansaldo Impianti
Centro Sperimentale del Boschetto
Corso F.M. Perrone, 118
16161 Genova
ITALY
Attn: C. Bozzolo

Ansaldo Impianti
Via Gabriele D'Annunzio, 113
16121 Genova
ITALY
Attn: S. Grifoni

ASEA-ATOM
Department KRD
Box 53
S-721 04
Vasteras
SWEDEN
Attn: A. Kjellberg

ASEA-ATOM
Department TQD
Box 53
S-721 04
Vasteras
SWEDEN
Attn: T. Granberg

ASEA KABEL AB
P.O. Box 42 108
S-126 12
Stockholm
SWEDEN
Attn: B. Dellby

Atomic Energy of Canada, Ltd.
Chalk River Nuclear Laboratories
Chalk River, Ontario K0J 1J0
CANADA
Attn: G. F. Lynch

Atomic Energy of Canada, Ltd.
1600 Dorchester Boulevard West
Montreal, Quebec H3H 1P9
CANADA
Attn: S. Nish

Bhabha Atomic Research Centre
Health Physics Division
BARC
Bombay-85
INDIA
Attn: S. K. Mehta

British Nuclear Fuels Ltd.
Springfields Works
Salwick, Preston
Lancs
ENGLAND
Attn: W. G. Cunliff, Bldg 334

Brown Boveri Reaktor GMBH
Postfach 5143
D-6800 Mannheim 1
WEST GERMANY
Attn: R. Schemmel

Bundesanstalt fur Materialprufung
Unter den Eichen 87
D-1000 Berlin 45
WEST GERMANY
Attn: K. Wundrich

CEA/CEN-FAR
Departement de Surete Nucleaire
Service d'Analyse Fonctionnelle
B.P. 6
92260 Fontenay-aux-Roses
FRANCE
Attn: M. Le Meur
J. Henry

CERN
Laboratorie 1
CH-1211 Geneve 23
SWITZERLAND
Attn: H. Schonbacher

Canada Wire and Cable Limited
Power & Control Products Division
22 Commercial Road
Toronto, Ontario
CANADA M4G 1Z4
Attn: Z. S. Paniri

Commissariat a l'Energie Atomique
ORIS/LABRA
BP N° 21
91190 Gif-Sur-Yvette
FRANCE
Attn: G. Gaussens
J. Chenion
F. Carlin

Commissariat a l'Energie Atomique
CEN Cadarche DRE/STRE
BP N° 1
13115 Saint Paul Lez Durance
FRANCE
Attn: J. Campan

Conductores Monterrey, S. A.
P.O. Box 2039
Monterrey, N. L.
MEXICO
Attn: P. G. Murga

Electricite de France
Direction des Etudes et Recherches
1, Avenue du General de Gaulle
92141 CLAMART CEDEX
FRANCE
Attn: J. Roubault
L. Deschamps

Electricite de France
Direction des Etudes et Recherches
Les Renardieres
Boite Postale n° 1
77250 MORET SUR LORING
FRANCE
Attn: Ph. Roussarie
V. Deglon
J. Ribot

EURATOM
Commission of European Communities
C.E.C. J.R.C.
21020 Ispra (Varese)
ITALY
Attn: G. Mancini

FRAMATOME
Tour Fiat - Cedex 16
92084 Paris La Defense
FRANCE
Attn: G. Chauvin
E. Raimondo

Furukawa Electric Co., Ltd.
Hiratsuka Wire Works
1-9 Higashi Yawata - 5 Chome
Hiratsuka, Kanagawa Pref
JAPAN 254
Attn: E. Oda

Gesellschaft fur Reaktorsicherheit (GRS) mbH
Glockengasse 2
D-5000 Koln 1
WEST GERMANY
Attn: Library

Gesellschaft fur Reaktorsicherheit (GRS) mbH
Forschungsgelande
8046 Garching
WEST GERMANY
Attn: S. Gossner

Health & Safety Executive
Thames House North
Milbank
London SW1P 4QJ
ENGLAND
Attn: W. W. Ascroft-Hutton

ITT Cannon Electric Canada
Four Cannon Court
Whitby, Ontario L1N 5V8
CANADA
Attn: B. D. Vallillee

Imatran Voima Oy
Electrotechn. Department
P.O. Box 138
SF-00101 Helsinki 10
FINLAND
Attn: B. Regnell
K. Koskinen

Institute of Radiation Protection
Department of Reactor Safety
P.O. Box 268
00101 Helsinki 10
FINLAND
Attn: L. Reiman

Instituto de Desarrollo y Diseno
Ingar - Santa Fe
Avellaneda 3657
C.C. 34B
3000 Santa Fe
REPUBLICA ARGENTINA
Attn: N. Labath

Japan Atomic Energy Research Institute
Takasaki Radiation Chemistry
Research Establishment
Watanuki-machi
Takasaki, Gunma-ken
JAPAN
Attn: N. Tamura
K. Yoshida

Japan Atomic Energy Research Institute
Tokai-Mura
Naka-Gun
Ibaraki-Ken
319-11
JAPAN
Attn: Y. Koizumi

Japan Atomic Energy Research Institute
Osaka Laboratory for Radiation Chemistry
25-1 Mii-Minami machi,
Neyagawa-shi
Osaka 572
JAPAN
Attn: Y. Nakase

Kraftwerk Union AG
Department R361
Hammerbacherstrasse 12 + 14
D-8524 Erlangen
WEST GERMANY
Attn: I. Terry

Kraftwerk Union AG
Section R541
Postfach: 1240
D-8757 Karlstein
WEST GERMANY
Attn: W. Siegler

Kraftwerk Union AG
Hammerbacherstrasse 12 + 14
Postfach: 3220
D-8520 Erlangen
WEST GERMANY
Attn: W. Morell

Motor Columbus
Parkstrasse 27
CH-5401
Baden
SWITZERLAND
Attn: H. Fuchs

NOK AG Baden
Beznau Nuclear Power Plant
CH-5312 Doettingen
SWITZERLAND
Attn: O. Tatti

Norsk Kabelfabrik
3000 Drammen
NORWAY
Attn: C. T. Jacobsen

Nuclear Power Engineering Test Center
6-2, Toranomon, 3-Chome
Minato-ku
No. 2 Akiyana Building
Tokyo 105
JAPAN
Attn: S. Maeda

Ontario Hydro
700 University Avenue
Toronto, Ontario M5G 1X6
CANADA
Attn: R. Wong
B. Kukreti

Oy Stromberg Ab
Helsinki Works
Box 118
FI-00101 Helsinki 10
FINLAND
Attn: P. Paloniemi

Rheinisch-Westfallscher
Technischer Uberwachunge-Vereln e.V.
Postfach 10 32 61
D-4300 Essen 1
WEST GERMANY
Attn: R. Sartori

Sydkraft
Southern Sweden Power Supply
21701 Malmo
SWEDEN
Attn: O. Grondalen

UKAEA
Materials Development Division
Building 47
AERE Harwell
OXON OX11 ORA
ENGLAND
Attn: D. C. Phillips

United Kingdom Atomic Energy Authority
Safety & Reliability Directorate
Wigshaw Lane
Culcheth
Warrington WA3 4NE
ENGLAND
Attn: M. A. H. G. Alderson

Waseda University
Department of Electrical Engineering
4-1 Ohkubo-3, Shinjuku-ku
Tokyo
JAPAN
Attn: K. Yahagi

1200	G. Yonas
1234	J. Chang/G. J. Lockwood
1800	R. L. Schwoebel
1810	R. G. Kepler
1811	L. A. Harrah
1811	R. L. Clough
1812	K. T. Gillen
1813	J. G. Curro
1815	R. T. Johnson
2155	J. E. Gover
2155	O. M. Stuetzer
2321	D. McKeon
2341	M. B. Murphy
5200	W. C. Myre
6200	V. L. Dugan
6300	R. W. Lynch
6400	A. W. Snyder
6410	J. W. Hickman
6420	J. V. Walker
6432	D. D. Carlson
6440	D. A. Dahlgren
6442	W. A. Von Riesemann
6444	S. L. Thompson
6445	B. E. Bader
6445	L. D. Bustard
6445	C. M. Craft
6446	L. L. Bonzon (20)
6446	W. H. Buckalew
6446	J. W. Grossman
6446	D. B. Hente
6446	F. V. Thome
6446	F. J. Wyant
6447	D. L. Berry
6449	K. D. Bergeron
6450	J. A. Reuscher
6450A	J. Bryson
6452	M. Aker/J. S. Philbin
8424	M. A. Pound
3141-1	C. M. Ostrander (5)
3151	W. L. Garner (3)

NRC FORM 335 (6-83) U.S. NUCLEAR REGULATORY COMMISSION

BIBLIOGRAPHIC DATA SHEET

1 REPORT NUMBER (Assigned by TIDC, add Vol. No., if any)
NUREG/CR-3643
SAND83-2493

2 Leave blank

3 TITLE AND SUBTITLE
Heterogeneous Oxidative Degradation in Irradiated Polymers

4 RECIPIENT'S ACCESSION NUMBER

5 DATE REPORT COMPLETED
MONTH: April YEAR: 1984

6 AUTHOR(S)
R. L. Clough
K. T. Gillen
C. A. Quintana

7 DATE REPORT ISSUED
MONTH: June YEAR: 1984

8 PERFORMING ORGANIZATION NAME AND MAILING ADDRESS (Include Zip Code)
Sandia National Laboratories
Albuquerque, New Mexico 87185

9 PROJECT/TASK/WORK UNIT NUMBER

10 FIN NUMBER
NRC FIN No. A-1051

11 SPONSORING ORGANIZATION NAME AND MAILING ADDRESS (Include Zip Code)
Division of Engineering Technology
Office of Nuclear Regulatory Research
U.S. Nuclear Regulatory Commission
Washington, DC 20555

12a TYPE OF REPORT

12b PERIOD COVERED (Inclusive dates)

13 SUPPLEMENTARY NOTES

14 ABSTRACT (200 words or less)

When polymeric materials are irradiated in the presence of air, oxygen-diffusion effects can, depending upon dose rate, lead to oxidative degradation which occurs only near the edges. This report describes the use of several recently developed techniques which are of general use for studying heterogeneous degradation in commercial polymeric materials. The techniques discussed are: optical evaluation of cross-sectioned, polished samples; cross-sectional profiling of changes in relative hardness; and profiling of density changes. Oxidation penetration depths are given for a number of major polymer types as a function of dose rate. A detailed example is given graphically illustrating the effects of differing oxidative penetration depths on the radiation-degradation behavior of a Viton® O-ring material; this particular material becomes hard and brittle when irradiated at high dose rate, but soft and stretchable when irradiated at low dose rates.

15a KEY WORDS AND DOCUMENT ANALYSIS

15b DESCRIPTORS

16 AVAILABILITY STATEMENT
Unlimited

17 SECURITY CLASSIFICATION (This report)
Unclassified

18 NUMBER OF PAGES
36

19 SECURITY CLASSIFICATION (This page)
Unclassified

20 PRICE
$